6 Crystallography

6-1 Charge Ordering of Eu_3S_4 Determined from the X-ray Valence Contrast between Eu^{2+} and Eu^{3+}

Eu_3S_4 is a mixed-valence compound and recognized as a unique system containing divalent rare-earth ions. It has a Th_3P_4-type structure with the space group of $I\bar{4}3d$ at room temperature, where divalent Eu^{2+} ($4f^7 5s^2 5p^6 6s^2$) and trivalent Eu^{3+} ($4f^6 5s^2 5p^6 5d^1 6s^2$) ions occupy a crystallographic site in a bcc lattice (Fig. 1a) [1]. The transport properties are characteristic of an intrinsic semiconductor, with the hopping of 4*f* electrons between adjacent Eu sites. The origin of the hopping motion of the charge carriers is considered as either thermally activated drift mobility or electron tunneling.

Eu_3S_4 has a non-magnetic phase transition at a temperature of T_c = 188.5 K as shown in Fig. 2 [2,3]. In Mössbauer spectra of $^{151}Eu_3S_4$ below T = 210 K, two absorption peaks were observed and interpreted as being due to electron hopping between Eu^{2+} and Eu^{3+} ions [4]. An X-ray powder diffraction study [7] found a 0.4% distortion in the ratio of *a/c* for the low-temperature phase. A charge-ordered tetragonal cell was topologically derived from the Th_3P_4 structure (Carter model) [5]. On the other hand, the failure to observe extra phonon modes in Raman scattering is inconsistent with the charge order-disorder transition model [6].

To understand the origin of the phase transition of Eu_3S_4, we have determined the crystal structure and cation distribution of Eu^{2+} and Eu^{3+} in the low-temperature phase by a single-crystal X-ray diffraction study [7]. The growth of twinned crystals was avoided by cooling with a magnetic field.

Fig. 1(b) shows a (001)-projection of the crystal structure of the low-temperature phase of Eu_3S_4 determined at T = 160 K. The crystal symmetry is tetragonal with a space group of $I\bar{4}2d$ and the cell dimensions are a = 8.508 ± 0.001 Å and c = 8.514 ± 0.002 Å. The crystal structure has two different kinds of Eu sites, defined as 4*a* and 8*d* sites, which can both be well represented by the Carter model [5]. Both Eu sites coordinate eight sulfur atoms, where the EuS_8 polyhedra are similar to the distorted cube of the room-temperature phase. Making a comparison between Fig. 1(a) and 1(b), it is clearly seen that the Eu ions maintain similar surroundings with sulfur through the phase transition.

X-ray intensity measurements for valence-difference contrast (VDC) analyses were made using a spherical single crystal at BL-10A. Wavelength slightly longer than the L_{II} absorption edge of Eu were selected for the VDC

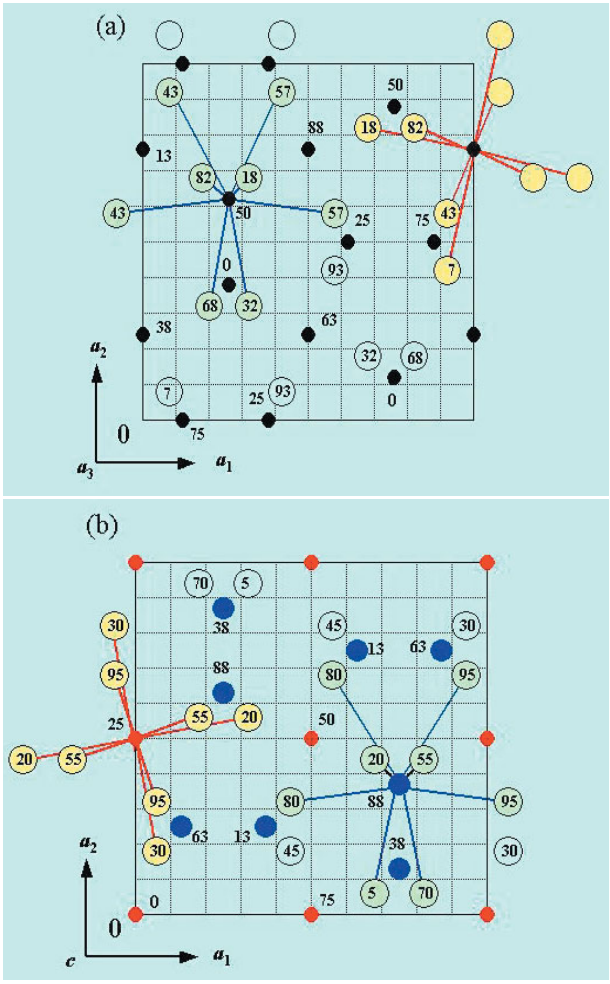

Figure 1
Crystal-structure projection of (a) room-temperature (T = 300 K) and (b) low-temperature (T = 160 K) phases of Eu_3S_4. (a) Black solid circle = Eu (12*a* sites), open circle = S (16*c*), (b) red solid circle = Eu (4*a*), blue solid circle = Eu (8*d*), open circle = S (16*e*). The heights of the atoms on the projection axis are given by integers, which should be multiplied by 100.

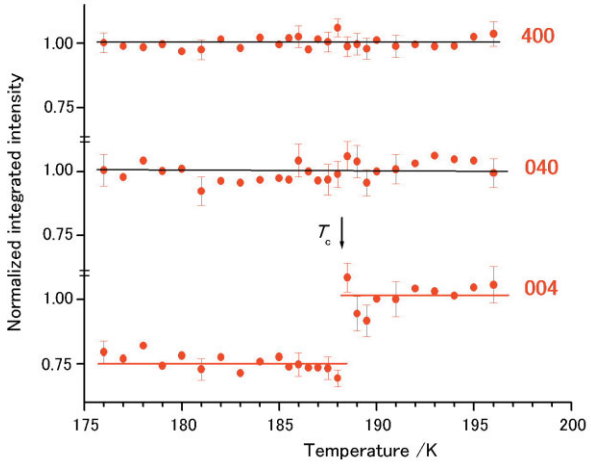

Figure 2
Temperature dependence of the 400, 040 and 004 Bragg intensities of Eu_3S_4. A discontinuity at T_c = 188.5 K can be observed only for the 004 reflection.

method, in order to keep a large difference in *f'* between Eu^{2+} and Eu^{3+} but the absorption effect small. Measurements of X-ray absorption near edge structure (XANES) spectra were performed at BL-3A to estimate the experimental-base *f'* values from *f''* and the Kramers-Krönig's dispersion relation.

The cation distribution of Eu^{2+} and Eu^{3+} was determined by crystal-structure analyses based on the intensity data collected at wavelengths of λ = 1.6312 and 1.6298 Å. Least-squares structural refinements suggest that the most plausible atomic arrangement is $[Eu^{3+}]^{4a}[Eu^{2+}Eu^{3+}]^{8d}S_4$. The variation of residual factors is plotted in Fig. 3 as a function of Eu^{2+} content in 4*a* sites. The curve of the residual factors has a minimum, which is close to zero for the occupancy of Eu^{2+} ions at 4*a* sites. This implies that Eu^{2+} ions do not occupy the 4*a* sites. Namely, the charge-ordering scheme is that a half of the Eu^{3+} ions occupy the whole 4*a* sites, while the remaining half of the Eu^{3+} ions mix with Eu^{2+} in 8*d* sites.

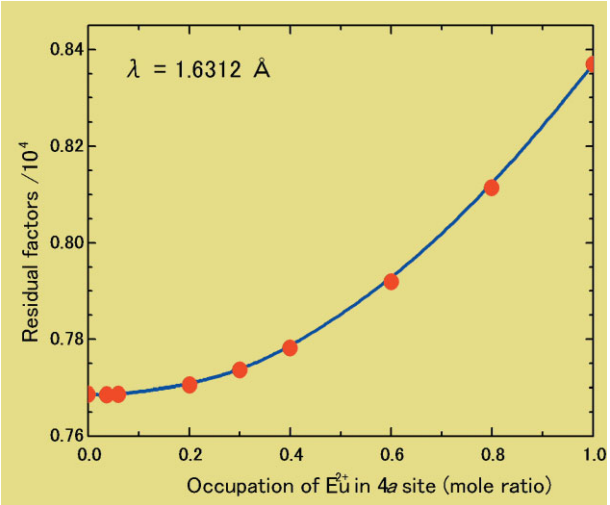

Figure 3
Residual factors in the refinements with the Synchrotron X-ray data measured at λ = 1.6312 Å and *T* = 180 K, given as a function of the mole ratio of Eu^{2+} ions occupied in the 4*a* sites in the $I\bar{4}2d$ structure.

S. Sasaki and H. Ohara (Tokyo Inst. of Tech.)

References

[1] K. Meisel and Z. Anorg, *Allgem. Chem.*, **240**, (1939) 300.
[2] I. Bransky, N. M. Tallan and A. Z. Hed, *J. Appl. Phys.*, **41**, (1970) 1787.
[3] Y. Konoike, T. Toyoda, K. Yamawaki and S. Sasaki, *Proc. Sympo. Atomic-Scale Surf. Interf. Dynam.*, **4**, (2000) 437.
[4] O. Berkooz, M. Malamud and S. Shtrikman, *Solid State Comm.*, **6**, (1968) 185.
[5] F.L. Carter, *J. Solid State Chem.*, **5**, (1972) 300.
[6] G. Güntherodt and W. Wichelhaus, *Solid State Commun.*, **39**, (1981) 1147.
[7] H. Ohara, S. Sasaki, Y. Konoike, T. Toyoda, K. Yamawaki and M. Tanaka, *Physica B,* **350**, (2004) 353.

6-2 Partial Charge Ordering in the $LiMn_2O_4$ Spinel

Lithium manganese spinels are attractive candidates for the cathode materials of rechargeable lithium ion batteries and have the advantages of low cost and low toxicity compared to cobalt- or nickel-containing oxides. Stoichiometric $LiMn_2O_4$ is believed to be a mixed valence compound in which distinct Mn^{3+} and Mn^{4+} ions are randomly distributed among the 16*d* sites of $Fd\bar{3}m$ symmetry (octahedral sites of spinel structure) [1-3]. This compound presents a first-order structural phase transition at 290 K, adopting a high temperature ideal cubic phase (*a* = 8.2468 Å, $Fd\bar{3}m$) above the transition and a low-temperature orthorhombic phase (3*a*×3*a*×*a*, *Fddd*) below [4,5]. The resistivity sharply increases by an order of magnitude at 290 K, showing similarity to the Verwey transition seen in Fe_3O_4. As is the case with the Verwey transition, which can be explained by the charge ordering of Fe^{2+} and Fe^{3+} on octahedral sites, the phase transition in $LiMn_2O_4$ has also explained by a partial charge ordering of Mn sites [4,5]. The structure of the low-temperature phase was first determined by powder neutron diffraction [4], however, high precision single-crystal X-ray diffraction experiments with synchrotron radiation can provide more accurate structural information including electron density distributions.

The experiments presented here were carried out using a horizontal-type four-circle diffractometer at BL-14A [6]. An eight-channel avalanche photodiode detector was used for photon counting [7]. The flux-grown $LiMn_2O_4$ crystal showed a first order phase transition at 294 K on cooling and at 310 K on heating. In all, 10732 reflections were measured in a reciprocal hemisphere up to 2θ = 73° at 297 K on heating, resulting in R/Rw = 0.038/0.038 for 1549 independent reflections [8].

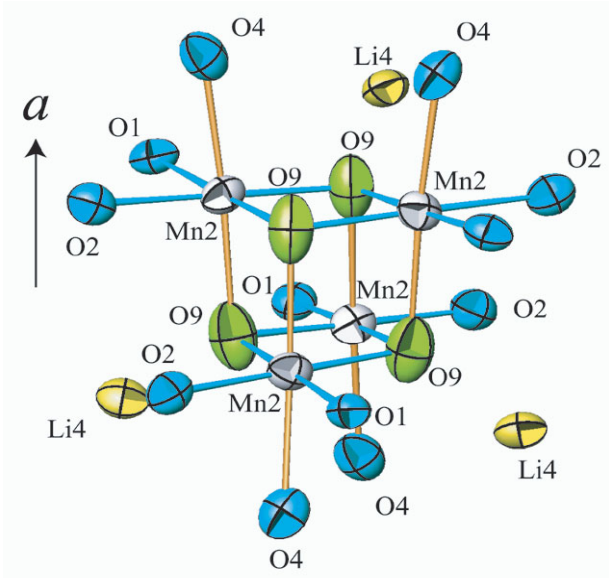

Figure 4
The distorted cube with a point symmetry of 222 formed by Mn2 and O9. Elongated and contracted Mn2-O bonds due to the Jahn-Teller distortion are shown in brown and blue, respectively.

In the derived structure there are five independent MnO_6 octahedra. Three of them have a tetragonal distortion, which was considered as a manifestation of the Jahn-Teller effect typical for the high spin Mn^{3+} cation. The remaining two have no such distortion. The bond valence sum (BVS) was calculated to be 3.06, 3.34, and 3.12 for Mn1, Mn2 and Mn3, and to be 3.89 and 3.88 for Mn4 and Mn5. Thus it is clear that a charge ordering does occur in the low temperature orthorhombic modification of $LiMn_2O_4$. However the number of Mn sites is not conformable to the 1:1 ordering of Mn^{3+} and Mn^{4+}, a necessary condition for charge neutrality. Actually, the slightly enhanced BVS value for Mn2 (3.34) suggests that a possible mixing of Mn^{3+} and Mn^{4+} may occur at Mn2 sites. In addition, we observed a large anisotropy of the atomic displacement parameter for O9, which forms a distorted cube with Mn2 cations as shown in Fig. 4. The thermal ellipsoid of O9 extends along the same direction as the tetragonal elongation of $Mn2O_6$ octahedron. This is considered to be further evidence of mixing valency at Mn2 sites.

Fig. 5 shows the distribution of elongated Mn-O bonds due to the Jahn-Teller distortion. It is notable that all the elongated Mn2-O bonds lie almost parallel to the *a*-axis, Mn3-O to the *b*-axis, and Mn1-O to the c-axis. Since the Mn2 site has a slightly mixed character in the oxidation state compared with Mn3, it is natural to think that Mn2-O along the *a*-axis is less elongated than Mn3-O along the *b*-axis. The orthorhombicity (a small difference between *a* and *b* lengths) can thus be interpreted as a manifestation of the Mn-O bond character.

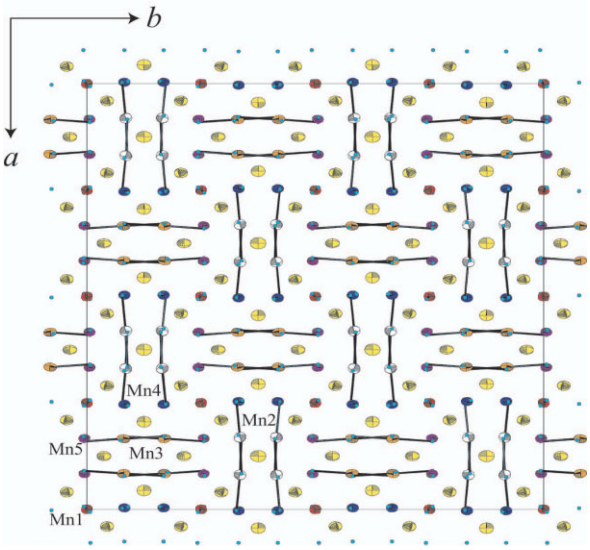

Figure 5
Distribution of Mn-O bonds elongated along the d_{z^2} orbital direction due to the Jahn-Teller distortion. Plotted: Mn1(red), Mn2(white), Mn3(orange), Mn4(blue), Mn5(purple), Li(yellow), O(tiny circle in pale blue).

K. Tateishi[1] and N. Ishizawa[2] ([1]Tokyo Inst. of Tech., [2]Ceramic Res. Lab. Nagoya Inst. of Tech.)

References

[1] K. Tateishi, D. du Boulay, N. Ishizawa and K. Kawamura, *J. Solid. State. Chem.,* **174**, (2003) 175.
[2] K. Tateishi, D. du Boulay and N. Ishizawa, *Appl. Phys. Lett.*, **84**[4], (2004) 529.
[3] K. Tateishi, D. du Boulay and N. Ishizawa, *J. Ceram. Soc. Japan, Suppl.*, **112**, (2004) S658.
[4] J. Rodríguez-Carvajal, G. Rousse, C. Masquelier and M. Hervieu, *Phys. Rev. Lett.*, **81**, 4660 (1998).
[5] G. Rousse, C. Masquelier, J. Rodríguez-Carvajal and M. Hervieu, *Electrochemical and Solid-State Lett.,* **2**, (1999) 6.
[6] Y. Satow and Y. Iitaka, *Rev. Sci. Instrum.*, **60**, (1989) 2390.
[7] S. Kishimoto, N. Ishizawa and T. P. Vaalsta, *Rev. Sci. Instrum.*, **69**, (1998) 384).
[8] K.Tateishi, K. Suda, D. du Boulay, N. Ishizawa and S. Oishi, *Acta Cryst. E,* **60**, (2004) i18.